Monte Carlo Calculation of Resonance Yield Curves and Resonance Energy Determination*

D. W. PALMER, J. G. SKOFRONICK, D. G. COSTELLO, A. L. MORSELL, W. E. KANE,† AND R. G. HERB
University of Wisconsin, Madison, Wisconsin
(Received 28 September 1962)

Yield curves for the $Al^{27}(p,\gamma)Si^{28}$ reaction at 992 keV have been studied extensively for thick and thin targets. Thick-target curves show a peak a few hundred eV above the resonance energy due to the discrete nature of energy losses suffered by protons as they penetrate the target. Theoretical thick- and thin-target yield curves have been obtained for this resonance by Monte Carlo calculations. Effects produced by discrete energy losses, by target contamination, and by nonuniform target thickness are investigated. Theoretical fits to experimental data for aluminum indicate that target contamination plays a major role in determining the shape of experimental thick-target yield curves. Experimental thick-target yield curves for the $Ni^{58}(p,\gamma)Cu^{59}$ resonances at 1424 and 1844 keV exhibit peaks in qualitative agreement with those predicted for other resonances by Monte Carlo calculations.

INTRODUCTION

THICK-TARGET yield curves exhibit a peak slightly above the resonance energy which has been called the Lewis peak.[1,2] As described previously, Monte Carlo methods have been used to fit such thick-target curves for the $Al^{27}(p,\gamma)Si^{28}$ resonance at about 992 keV.[2] A more general Monte Carlo computer program has now been designed which can be used for pure and contaminated, thick and thin targets. This program is described in the present paper, and yield curves calculated with it are compared with recent experimental data.

THE LEWIS PEAK

To understand the occurrence of the Lewis peak, one must recall that a charged particle in passing through a target loses energy in discrete steps, Q, due to Coulombic collisions with electrons of the target media.[3] For heavy, nonrelativistic particles, the energy losses are assumed to be distributed as $1/Q^2$ between a maximum, Q_{max}, corresponding to a head-on collision, and a minimum, $Q_{min}=I^2/Q_{max}$, where I is the geometric mean of ionization and excitation energies of the stopping material.[4] Figure 1 traces out the paths of two typical particles which enter the target at the same energy E_i. The number of resonance reactions produced is proportional to the total distance the particles travel while in the resonance region. When E_i is above the resonance, a particle may jump completely over it if the resonance is sufficiently narrow and, thus, will not contribute to the yield; when E_i is at the resonance energy, however, all particles have a chance to interact. This accounts for the Lewis peak.

If many paths are generated, such as in Fig. 1, which are consistent with the physical laws, then the shape of resonance yield curves can be predicted. Monte Carlo techniques are ideal for this task.

PROCEDURE

Resonance Yield

In describing the Monte Carlo program, it is convenient to begin by considering an expression for the

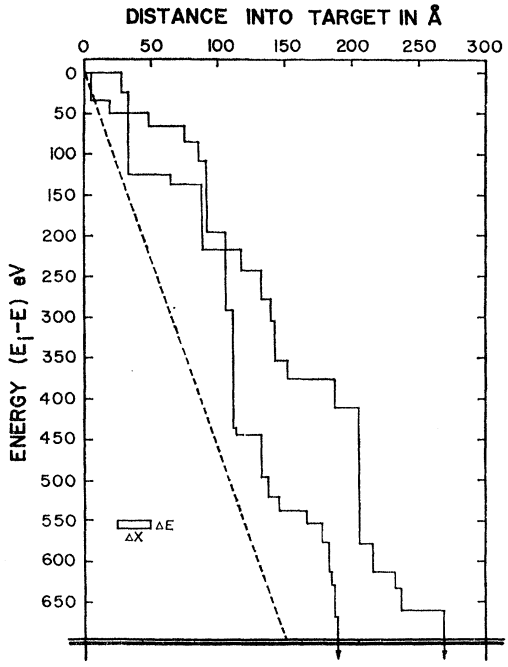

FIG. 1. Monte Carlo calculated trajectories for two protons in aluminum at 1 MeV. Proton energy E is plotted relative to incident energy E_i. Dashed line indicates path expected if energy losses were in infinitesimal increments. Rectangles of dimensions ΔE, ΔX were used in the computer program.

* Work supported by the U. S. Atomic Energy Commission and the Wisconsin Alumni Research Foundation.
† Present address: Lawrence Radiation Laboratory, University of California, Livermore, California.
[1] W. L. Walters, D. G. Costello, J. G. Skofronick, D. W. Palmer, W. E. Kane, and R. G. Herb, Phys. Rev. Letters **7**, 284 (1961).
[2] W. L. Walters, D. G. Costello, J. G. Skofronick, D. W. Palmer, W. E. Kane, and R. G. Herb, Phys. Rev. **125**, 2012 (1962).
[3] Recently, H. W. Lewis noticed a 1946 paper by G. Placzek and asked that we call attention to it. Placzek [Phys. Rev. **69**, 422 (1946)] works out the distribution in energy of initially monoenergetic neutrons as they pass through matter. Results are similar in form to results obtained by Lewis for charged particles.
[4] F. Bloch, Z. Physik **81**, 363 (1938).

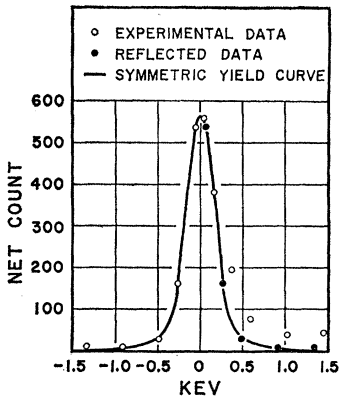

FIG. 2. Symmetric yield curve for protons on aluminum target 60 eV thick (reference 5). High-energy half of the curve was formed by reflection of low-energy half through the peak.

number of reactions produced when N particles are incident on a target of thickness t having a resonance at energy E_R:

$$Y(E_B,t)=N\int_0^\infty dE\,\sigma(E)\int_0^\infty dE_i\,g(E_B,E_i)\times\int_0^t dx\,W(E_i,E,x)n(x), \quad (1)$$

where $\sigma(E)$ is a modified Breit-Wigner cross section which includes Doppler broadening; $g(E_B,E_i)$ is the normalized energy distribution in incident energy for the particles with mean energy E_B; $W(E_i,E,x)dE$ is the probability that a particle incident at energy E_i will have energy between E and $E+dE$ at a distance x in the target; and $n(x)$ is the number of disintegrable nuclei/cm^3, which will depend on x for a contaminated target. Equation (1) is a rather cumbersome expression for the yield, and considerable simplification is possible.

The function $W(E_i,E,x)$ depends energy-wise only on the difference E_i-E as long as the stopping mechanism does not vary over the energy range considered. Further, we may assume that $g(E_B,E_i)$ depends on E_B-E_i. These assumptions and some additional manipulations (see Appendix A) using the change of variables $\epsilon=E_i-E$ lead to the equation

$$Y(E_B,t)\propto N\int_0^\infty d\epsilon\,Y(E_B-\epsilon,0)\int_0^t dx\,W(\epsilon,x)n(x), \quad (2)$$

where $Y(E_B-\epsilon,0)$ is the yield from a target of infinitesimal thickness. Equation (2) may be approximated by breaking up the ranges in ϵ and x into intervals of width $\Delta\epsilon$ and Δx, respectively, and by replacing the integrals by sums to arrive at

$$Y(E_B,t)\propto N\sum_i \mathcal{Y}_i\sum_{j=1}^m W_{ij}n_j\Delta x\Delta\epsilon, \quad (3)$$

where $\mathcal{Y}_i$ is the value of $Y(E_B-\epsilon,0)$ somewhere inside the energy interval i, and W_{ij} is the value of $W(\epsilon,x)$ somewhere inside the energy-distance rectangle (i,j). The probability W_{ij} vanishes at large i for targets of finite thickness $t=m\Delta x$, and then the sum over i extends to all nonvanishing values of the product $\mathcal{Y}_iW_{ij}$. We may now define a new quantity $L_{ij}=NW_{ij}\Delta x\Delta\epsilon$, which is the total track length traveled by the particles in rectangle (i,j). With this substitution, the yield becomes

$$Y(E_B,t)\propto\sum_i \mathcal{Y}_i\sum_{j=1}^m L_{ij}n_j. \quad (4)$$

This expression is used for the yield throughout this paper. In practice, the $\mathcal{Y}_i$'s are obtained from an experimental yield curve for a very thin target; the L_{ij}'s are generated by Monte Carlo methods with the aid of a computer; and n_j is set equal to one for a pure target, so that it gives the fraction of disintegrable nuclei present in layer j of the target.

Equation (4) can be understood more readily by realizing that the sums $\sum_{j=1}^m L_{ij}n_j$, $i=1, 2, \cdots$ give the energy distribution inside the target for particles which initially are monoenergetic, each layer j being weighed according to the density of disintegrable nuclei. This statement is true for a range in E which is small compared to E_i. If the resonance were a delta function, these sums would give the shape of the yield curve produced with a beam of infinite resolution. Spreading factors such as resonance width, Doppler broadening, and finite beam resolution are included by folding these sums into the $\mathcal{Y}_i$'s, which are the yield values for a target of infinitesimal thickness. This folding process is prescribed in Eq. (4).

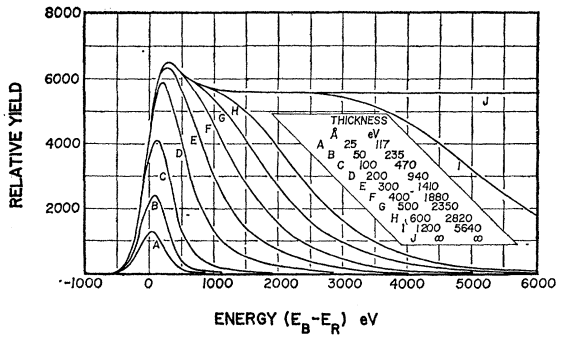

FIG. 3. Monte Carlo calculated yield curves for the $Al^{27}(p,\gamma)Si^{28}$ resonance at 992.4 keV. Target thickness in Å and eV is indicated (reference 5). To produce these curves, the thin-target yield curve in Fig. 2 was folded into proton energy distribution curves as determined by a computer. Resolution ≈4000. Thick-target peak-to-plateau ratio = 1.16.

[5] Target thickness in eV is the average energy lost in the target by 992.4-keV protons.

Monte Carlo Program

To obtain the L_{ij}'s, the target is subdivided into energy-distance rectangles such as depicted in Fig. 1. A computer then follows each charged particle through

successive collisions in the target by generating pairs of random numbers which determine the path length and energy loss for each collision. The track length in each rectangle (i,j) through which it passes is recorded. When a particle has lost energy corresponding to a preassigned amount, another particle is tracked in like fashion adding in each rectangle its track length to those which preceded. This is done for N particles.

The distance traveled between collisions, X, is determined from a random number R by $X=-\lambda \ln(1-R)$, where λ is the mean path length, and the energy loss Q for a collision is determined from another random number R by $Q=Q_{\min}/[1-R(1-Q_{\min}/Q_{\max})]$. These equations distribute the path lengths exponentially and energy losses as $1/Q^2$, which is the approximation normally used for nonrelativistic, Coulombic collisions over an energy range small compared to the incident energy.

RESULTS

Ideal and Experimental Yield Curves

A Control Data Corporation 1604 digital computer was used for the Monte Carlo work. The computer was

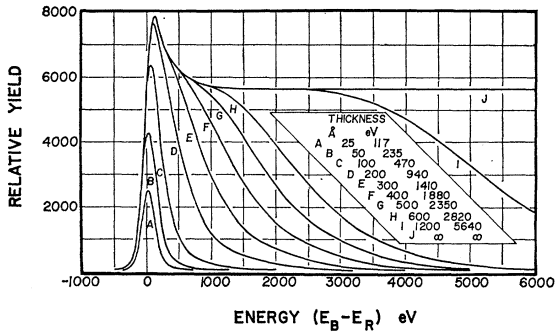

FIG. 4. Monte Carlo calculated yield curves for the $Al^{27}(p,\gamma)Si^{28}$ resonance at 992.4 keV. Target thickness in Å and eV is indicated (reference 5). To produce these curves, the thin-target yield curve in Fig. 2 with energy scale halved was folded into proton energy distribution curves as determined by a computer. Resolution $\approx$8000. Thick-target peak-to-plateau ratio=1.40.

run for 20 000 protons incident on aluminum at 992.4 keV with the intent of studying the $Al^{27}(p,\gamma)Si^{28}$ resonance at that energy. Values for the parameters used were $Q_{\min}=12.3$ eV,[6] $Q_{max}=2160$ eV, $\lambda=13.5$ Å,[7] $\Delta\epsilon=10$ eV, and $\Delta x=25$ Å. The output of the computer was the total track length L_{ij} in each of the rectangles (i,j).

To obtain the yield curve for a pure target of thickness t, n_j was set equal to 1 for all j values in Eq. (4), and the double summation $\sum_i Y_i \sum_{j=1}^{m} L_{ij} n_j$, $m=t/\Delta x$

[6] This value of $Q_{\min}$ was calculated from the expression $Q_{\min}=I^2/Q_{\max}$ where the value of $I=163$ eV was used as reported by Hans Bichsel and Edwin A. Uehling, Phys. Rev. **119**, 1670 (1960).

[7] This value for λ was obtained from the expression $K=Q_{av}/\lambda$, where $K=4.7$ eV/Å is the stopping power of 992-keV protons in aluminum, and Q_{av} is the mean energy loss calculated by assuming the $1/Q^2$ probability between the limits $Q_{\min}$ and $Q_{\max}$.

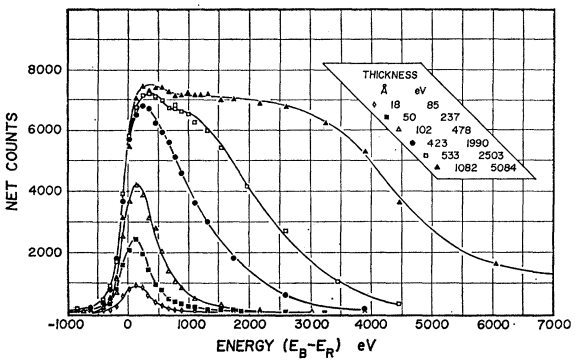

FIG. 5. Experimental yield curves for the $Al^{27}(p,\gamma)Si^{28}$ resonance at 992.4 keV. Beam energy E_B is plotted relative to resonance energy E_R. E_R was chosen such that the over-all appearance is like Fig. 3. Target thickness in Å and eV is indicated (reference 5). Each target was produced by evaporation of Al onto previous target inside target chamber. A yield curve was obtained after each deposition. Total elapsed time $\approx$24 h. Beam resolution $\approx$4000. Thick-target peak-to-plateau ratio=1.05.

was performed using values for Y_i determined by the experimental, thin-target yield curve shown in Fig. 2. Each of the curves in Fig. 3 was obtained in this manner. To produce the set of curves with higher resolution shown in Fig. 4, new values of Y_i, determined by arbitrarily halving the abscissa in Fig. 2, were inserted into Eq. (4).

These calculated curves should be compared with the two sets of curves in Figs. 5 and 6, which were obtained experimentally using protons from an electrostatic generator. The targets were produced inside the vacuum system of an all-metal target chamber by evaporating aluminum onto a tantalum backing. First, a thin target was evaporated and the yield curve determined. More aluminum was then evaporated onto the same target, and another yield curve was determined, and so on. Each set of curves was produced without interruption over a period of approximately

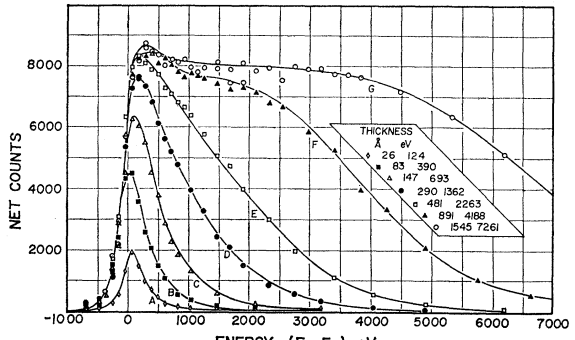

FIG. 6. Experimental yield curves obtained with a second set of targets for the $Al^{27}(p,\gamma)Si^{28}$ resonance at 992.4 keV. Beam energy E_B is plotted relative to resonance energy E_R. E_R was chosen such that the over-all appearance is like Fig. 3. Targets were produced, and yield curves were obtained as for curves of Fig. 5. Total elapsed time $\approx$24 h. Beam resolution $\approx$4000. Thick-target peak-to-plateau ratio=1.09.

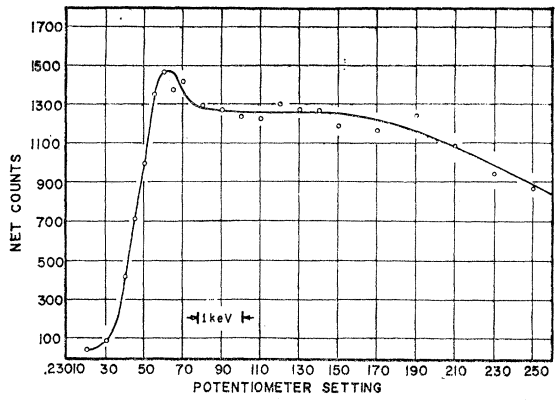

FIG. 7. Experimental thick-target yield curve for the $Al^{27}(p,\gamma)Si^{28}$ resonance at 992.4 keV. Beam resolution ≈8000. Peak-to-plateau ratio = 1.17. Target produced by evaporation of aluminum onto tantalum backing while in evacuated target chamber.

24 h. The target thickness in Å given for each experimental curve was determined by dividing the area under the curve by the stopping power and the plateau height of the thick-target yield curves. This quotient is the thickness of a pure target which has the same average number of active nuclei per cm^2 of surface as the actual target (see Appendix C). The applicability of this method was verified by applying it to the theoretical curves for targets of known thickness.

Salient features of these experimental and theoretical families are: (1) Thick-target curves show the predicted Lewis peak; (2) the energy at maximum yield shifts only slightly with increasing target thickness; (3) the curves show very great asymmetry; and (4) the energy position of half-plateau yield for the thick targets does not agree with the energy of maximum yield for the thinnest target.

Some experimental data have been taken at resolution $R = 8000$ on aluminum at 992.4 keV and nickel at 1424 and 1884 keV utilizing only thick targets. These yield curves are shown in Figs. 7, 8, and 9. The ratio of the peak-to-plateau yield for the aluminum in Fig. 7 has increased as expected for higher resolution. The peak-to-plateau ratios for the nickel resonances are considerably larger than that for the aluminum resonance with the same beam resolution. This result occurs because both Q_{min} and Q_{max} are larger for these resonances in nickel than for the aluminum resonance, so that the probability of a large energy loss in a single collision in nickel is increased.

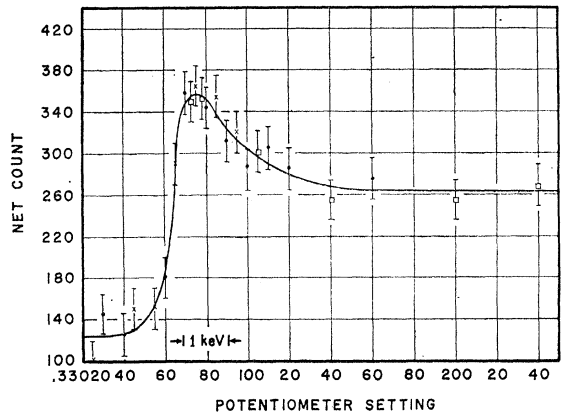

FIG. 8. Experimental thick-target yield curve for the $Ni^{58}(p,\gamma)Cu^{59}$ resonance at 1424 keV. Data points for four separate runs are shown. Resolution ≈8000. Peak-to-plateau ratio = 1.71. Target produced by evaporating nickel onto tantalum backing while in evacuated target chamber.

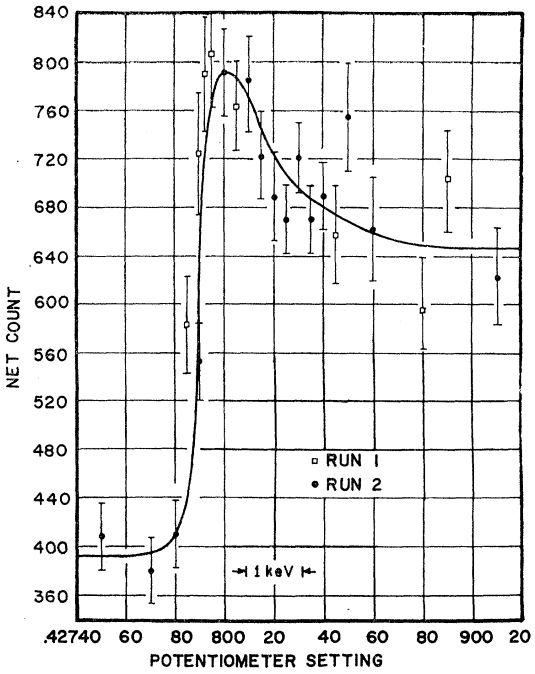

FIG. 9. Experimental thick-target yield curve for the $Ni^{58}(p,\gamma)Cu^{59}$ resonance at 1844 keV. Data points for two separate runs are shown. The same target was used for the curve in Fig. 8. Resolution ≈8000. Peak-to-plateau ratio = 1.56. Target produced by evaporation of nickel onto tantalum backing while in evacuated target chamber.

The effects on thick-target yield curves of varying Q_{min} and Q_{max} were explored with the Monte Carlo computer program. Figure 10 displays the energy distribution of initially monoenergetic protons for three pairs of values of Q_{min} and Q_{max}. These are normalized plots of the sum $\sum L_{ij}$ vs i; but as mentioned above, the energy distribution is given by these sums. Note that the largest Q_{min}, Q_{max} pair has the largest peak.[8]

Nonideal Targets

It has been observed experimentally that the peaks of the aluminum thick-target yield curves disappear with time, although the energy corresponding to half of the plateau yield remains relatively fixed. This fact,

[8] The authors would be pleased to send to any interested persons details of the Monte Carlo programs and the Monte Carlo results.

coupled with differences in shape between the Monte Carlo and experimental thin-target yield curves, several of which are compared in Fig. 11, suggests that the experimental targets may be quite different from the ideal targets considered so far.

Many nonideal target conditions can be studied with the L_{ij}'s of the Monte Carlo program. For example, foreign substances anywhere in or on the target in any proportion can be treated as well as rough surfaces on the target and on the target backing material. It is possible to study these conditions with the L_{ij}'s which were produced for a pure target. Equation (4) is used

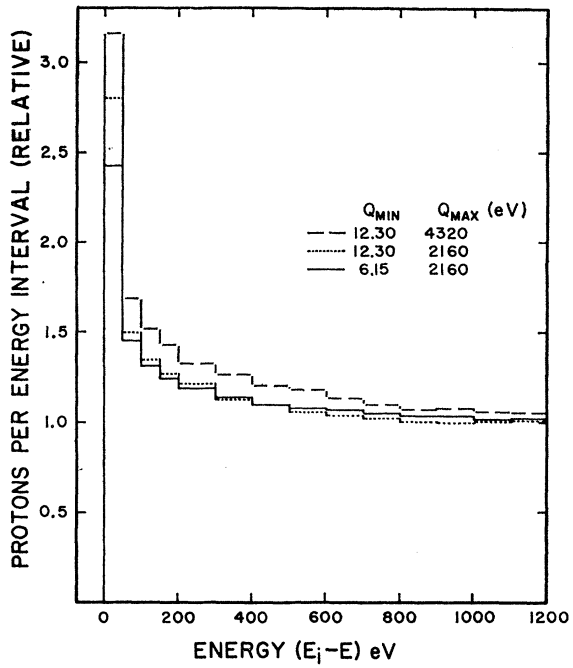

FIG. 10. Monte Carlo calculated proton energy distributions in targets with different Q_{min} and Q_{max} values. Q_{min} and Q_{max} are minimum and maximum energy loss allowed per collision, respectively. Energy interval size is arbitrary but constant. The distribution in aluminum at 992.4 keV is given by the 12.3, 2160 eV pair. Nickel at 1844 keV would correspond to approximately 25.8, 4014 eV Q values (reference 9). Other distributions obtained but not shown because of confusing overlap are for (1) 24.6, 4320 eV Q values which closely follows the 12.3, 4320 eV distribution except for an average value of 3.84 from 0–50 eV, and (2) the 24.6, 2160 eV distribution which closely follows the 12.3, 2160 eV distribution except for an average value of 3.37 from 0–50 eV.

again, but now the n_j's are less than one in contaminated layers. Thus, if $n_1=0$, and the remaining n_j's$=1$, the resulting yield curve would reveal the effects of a 25 Å layer of "aluminum-equivalent" contamination on the target surface—contamination which is distinguishable from aluminum only in that it does not produce gamma rays. The degree of correspondence between

[9] Minimum energy loss Q_{min} calculated from $Q_{min}=I^2/Q_{max}$ where, in eV, $I=11.5Z$ and Z is the atomic number of the stopping material.

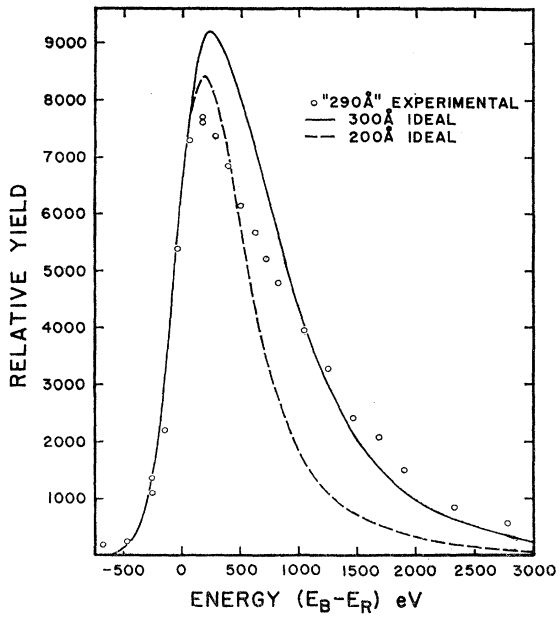

FIG. 11. Comparison of two Monte Carlo calculated yield curves for pure, uniform targets with experimental yield data for the 992.4-keV $Al^{27}(p,\gamma)Si^{28}$ resonance. Experimental data are the same as for 290 Å target in Fig. 6.

real contamination and "aluminum-equivalent" contamination will depend on the type of contamination.

Thick Targets

Figures 12 through 16 show some results of the contamination study on thick targets. The dashed curve in each figure is an experimental curve for which the peak has disappeared, and the goal was to fit this curve

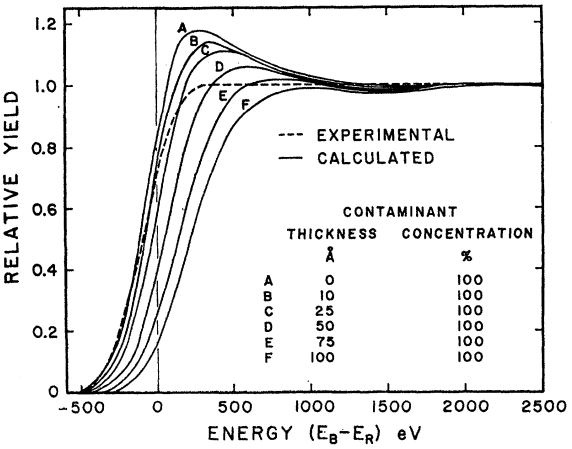

FIG. 12. Calculated thick-target 992.4-keV $Al^{27}(p,\gamma)Si^{28}$ yield with "aluminum-equivalent" contaminant layers of 100% concentration (reference 10). Dashed line indicates experimental curve to which fit is desired.

[10] "Aluminum-equivalent" contaminant differs from aluminum only in that it will not participate in a resonance reaction.

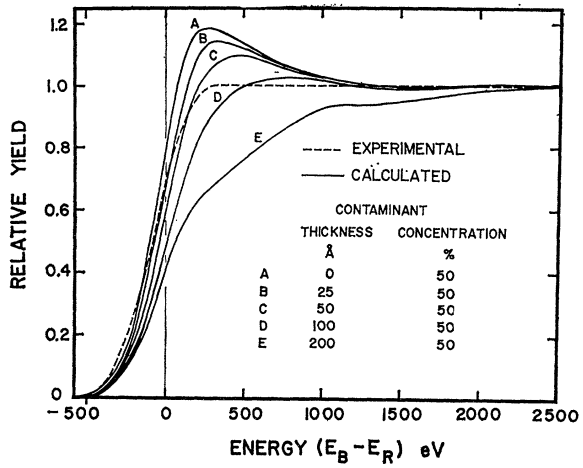

FIG. 13. Calculated thick-target 992.4-keV $Al^{27}(p,\gamma)Si^{28}$ yield with "aluminum-equivalent" contaminant of 50% concentration (reference 10). This may be a layer of contaminant covering 50% of the surface, or it may consist of the same amount of contaminant dispersed in the target with 50% concentration. Dashed line indicates experimental curve to which fit is desired.

as well as possible in hopes of learning what were the experimental target conditions. Figure 12 shows that a 100 Å layer of completely inert material on the target surface can reduce the peak-to-plateau ratio considerably, but it also shifts the energy for half-plateau yield to more than 300 eV above that of the experimental curve.

In Figs. 13 through 16, many contaminant configurations are possible for each of the yield curves. For example, in Fig. 16, a 50 Å, 15% contaminant distribution could be 50 Å lumps of contaminant covering 15% of the target surface, or, on the other extreme, contamination extending 50 Å into the target with 15% concentration. These distributions and intermediate ones give the same yield curve.

The yield curves in Fig. 13 again indicate too much

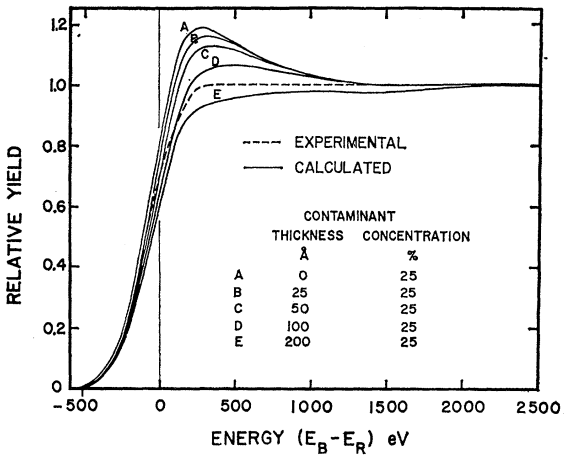

FIG. 14. Calculated thick-target 992.4-keV $Al^{27}(p,\gamma)Si^{28}$ yield with "aluminum-equivalent" contaminant of 25% concentration (reference 10). Dashed line indicates experimental curve to which fit is desired.

shift in the energy for half-plateau yield and thus do not agree with experiment. Agreement is obtained finally in curve *E* of Fig. 14, with 200 Å, 20% "aluminum-equivalent" contaminant. Thus, it appears that the Lewis peak will be eliminated while retaining the energy value at half-plateau yield if about 20% of the protons encounter contaminant atoms at any given depth up to 200 Å in the target. Whether the contaminant is distributed in lumps on the surface or uniformly in the target cannot be determined.

Thin Targets

Examination of the experimental and ideal thin-target yield curves in Fig. 11 reveals several marked differences: (1) Maximum yield for the experimental curve is less than expected for a pure target of uniform

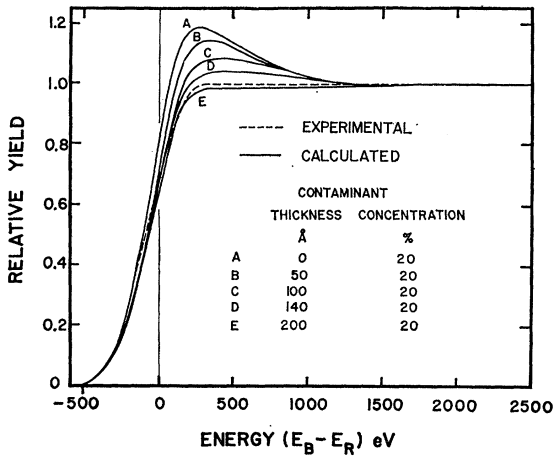

FIG. 15. Calculated thick-target 992.4-keV $Al^{27}(p,\gamma)Si^{28}$ yield with "aluminum-equivalent" contaminant of 20% concentration (reference 10). Dashed line indicates experimental curve to which fit is desired.

thickness; (2) the experimental curve exhibits more asymmetry than predicted; and (3) the peak of the experimental curve occurs at lower energy than expected. Each of these differences can be attributed to one of several causes. The reduced peak height of experimental curves, for example, may be due to nonuniform target thickness or target contamination.

Nonuniform target thickness could be brought about by either rough front or back surfaces, or both. To a beam of particles, however, rough front and back surfaces on targets such as shown schematically in Fig. 17 cannot be distinguished, and identical yield curves would result.

Figure 18 shows theoretical yield curves produced with the aid of Eq. (4) for targets shown schematically. All targets are pure and have the same average thickness, but they differ in the degree of irregularity in thickness. These yield curves demonstrate that with given average thickness, the more uneven targets reduce the maximum yield, increase the asymmetry, and can

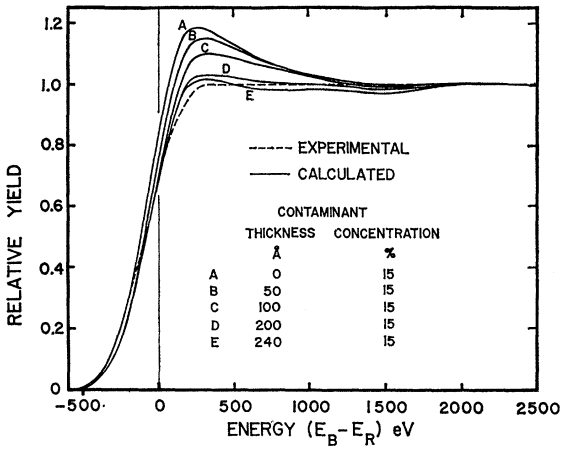

FIG. 16. Calculated thick-target 992.4-keV $Al^{27}(p,\gamma)Si^{28}$ yield with "aluminum-equivalent" contaminant of 15% concentration (reference 10). Dashed line indicates experimental curve to which fit is desired.

shift the peak to lower or higher energy. The areas under the curves are the same, as should be the case for targets of the same average thickness. (See Appendix B.)

The effects produced by introducing contamination on or in the target are even more pronounced, as Fig. 19 demonstrates. Just as for contaminated thick targets, the contaminant here could consist of lumps covering a portion of the target surface, as depicted in the figure; or, on the other extreme, the contaminant may be dispersed and distributed uniformly up to a depth in the target equal to the depth of the lumps. For "aluminum-equivalent" contamination, these two cases are equivalent. It can be seen from the figure that contamination reduces the peak height, increases the asymmetry, and does not affect the area. These effects were observed to occur for targets of nonuniform thickness, also. Now, however, the peak is shifted invariably toward higher energy.

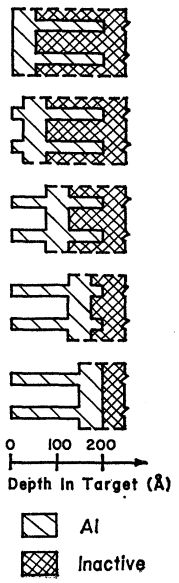

FIG. 17. Equivalent target configurations. Each target appears the same to an incoming beam of protons. Inactive material is the target backing plate.

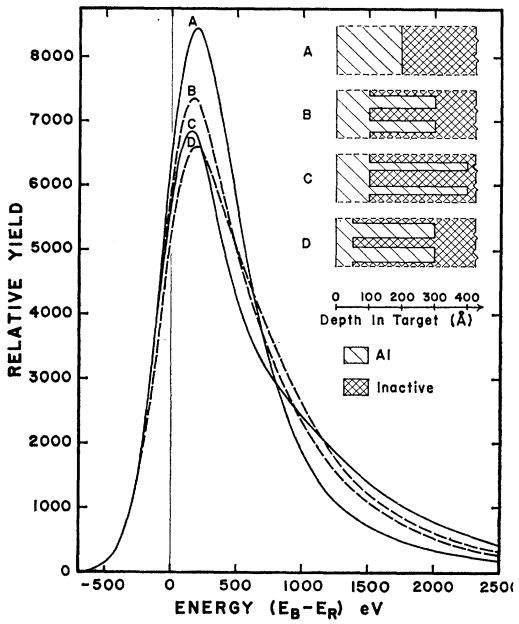

FIG. 18. Calculated 992.4-keV $Al^{27}(p,\gamma)Si^{28}$ yield for targets of nonuniform thickness. Target configuration indicated at right. All targets have 200 Å average thickness of pure aluminum. Inactive material is the target backing plate.

Theoretical fits have been obtained with the Monte Carlo work for some of the experimental, thin-target yield curves, Figs. 20 and 21. Surprisingly, no contamination was needed, as the blocks at the right in the figures indicate. The target conditions needed for these fits might have been predicted from Fig. 11 in view of what is now known of the effects of nonuniform target thickness and contamination.

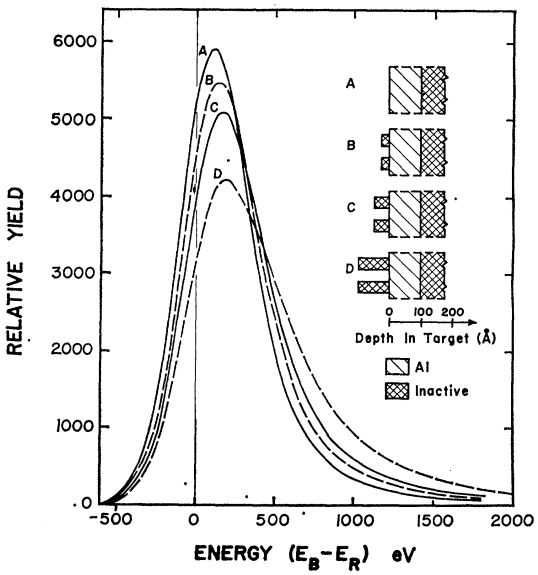

FIG. 19. Calculated 992.4-keV $Al^{27}(p,\gamma)Si^{28}$ yield for targets with contaminated surfaces. Target configuration indicated at right. Target backing also shown.

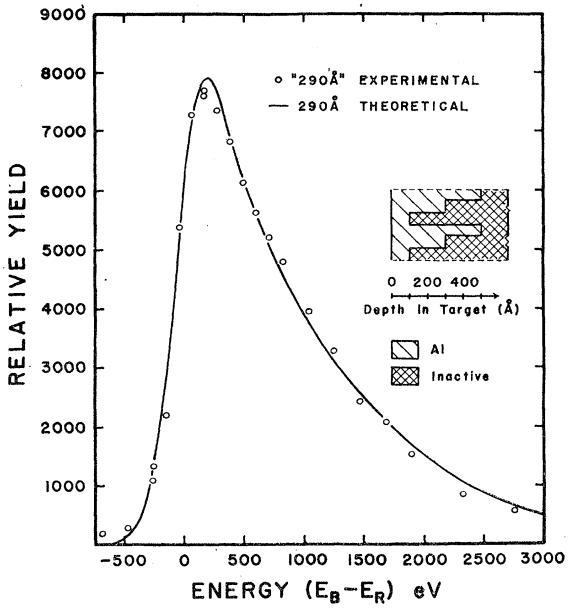

FIG. 20. Monte Carlo calculated fit to an experimental 992.4-keV $Al^{27}(p,\gamma)Si^{28}$ thin-target yield curve. Experimental curve is same as in Fig. 11. Target configuration used for theoretical fit is shown. (See Fig. 17.) Experimental and theoretical target have same average number of aluminum nuclei/cm². (See Appendix B.) Inactive material is target backing plate.

RESONANCE ENERGY

Three methods have been used in the past for locating the resonance energy from resonance yield curves: (1) for targets which are thin compared to the natural

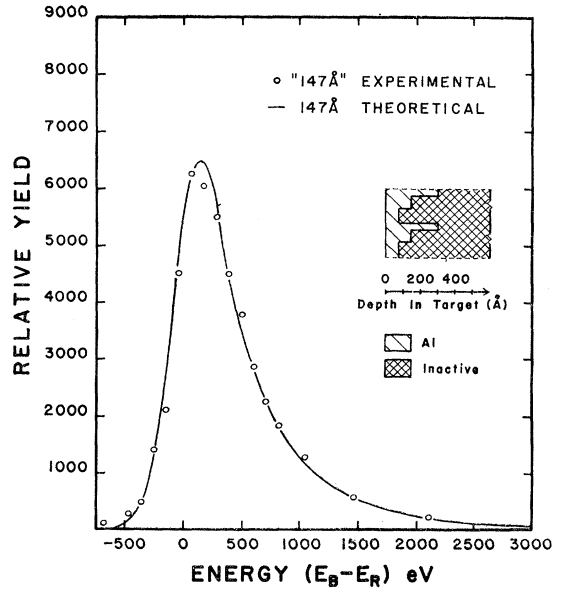

FIG. 21. Monte Carlo calculated fit to an experimental 992.4-keV $Al^{27}(p,\gamma)Si^{28}$ thin-target yield curve. Experimental curve is same as for 147 Å target in Fig. 6. Target configuration used for theoretical fit is shown. (See Fig. 17.) Experimental and theoretical targets have same average number of aluminum nuclei/cm². (See Appendix B.) Inactive material is the target backing plate.

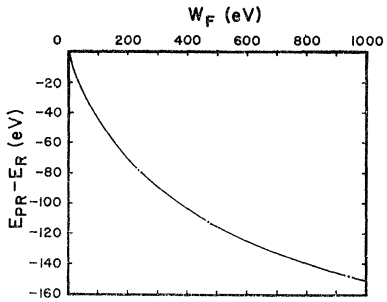

FIG. 22. Comparison of resonance energy E_R with energy at half-plateau yield E_{PR}. Points were taken from Monte Carlo calculated 992.4-keV $Al^{27}(p,\gamma)Si^{28}$ thick-target yield curves such as in Figs. 3 and 4. W_F indicates the magnitude of the spreading factors and equals the total width at half-maximum of the very thin-target yield curve corresponding to each point.

width of the resonance, Γ, the resonance has been assumed to correspond to the position of maximum yield; (2) for targets with thickness of the same order as Γ, the resonance energy was supposed to be located below the position of maximum yield by an amount equal to one-half of the target thickness in eV; and (3) for targets which are thicker than Γ, the resonance energy was supposed to be the energy corresponding to half-plateau yield.[11]

The last two methods could give correct results only if energy losses were in infinitesimal increments, and if the targets were uniform and pure. The first method, while valid with energy increments as they actually are, may produce values in error due to contaminant on the target surface and may be handicapped by poor statistics due to low yield. Since the location of the resonance is known for the Monte Carlo curves, these theoretical yield curves provide a good means of comparing the true resonance energy E_R with the values predicted by past methods E_{PR}.

For pure thick targets, the energy corresponding to half-plateau height depends on the resonance width,

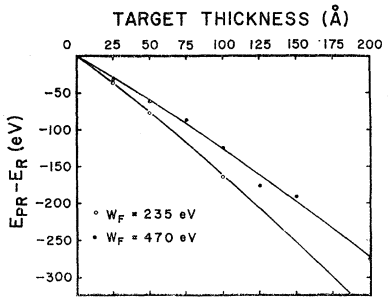

FIG. 23. Comparison of resonance energy E_R with E_{PR}, the energy at peak of thin-target yield curve less one-half of target thickness in eV. Points were taken from Monte Carlo calculated 992.4-keV $Al^{27}(p,\gamma)Si^{28}$ thick-target yield curves such as in Figs. 3 and 4. W_F indicates the magnitude of the spreading factors and equals the total width at half-maximum of the very thin-target yield curve corresponding to each point.

[11] W. A. Fowler, C. C. Lauritsen, and T. Lauritsen, Rev. Mod. Phys. **20**, 236 (1948).

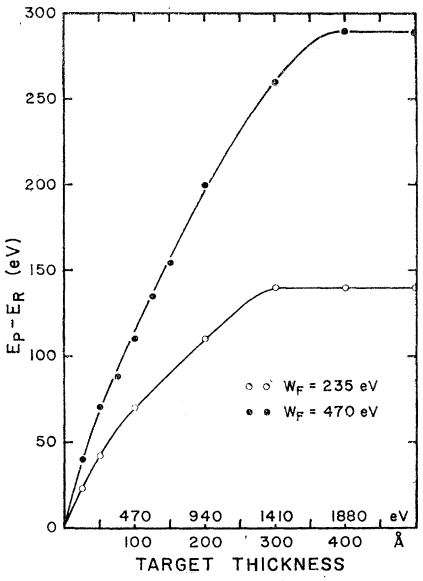

FIG. 24. Comparison of resonance energy E_R, with E_P, the energy at peak of thin-target yield curve. Points taken from Monte Carlo calculated 992.4-keV $Al^{27}(p,\gamma)Si^{28}$ yield curves such as in Figs. 3 and 4. W_F indicates the magnitude of spreading factors and equals the total width at half-maximum of the very thin-target yield curve corresponding to each point.

beam resolution, and Doppler broadening, the same factors which determine the width of a very thin target yield curve. Since the Monte Carlo curves were calculated using a very thin target yield curve, its full width at half-maximum, W_F, is a good measure of these spreading factors. Figure 22 shows how the resonance energy predicted by method 3 depends on W_F.

Method 2 was applied to the Monte Carlo curves in Figs. 3 and 4, and E_{PR}, the resonance energy predicted, was found to vary considerably with target thickness, as shown in Fig. 23. Some dependence on the spreading factors, W_F, is shown also.

To determine the resonance energy experimentally, comparison of experimental and theoretical yield curves may be useful. Figure 24 shows for the aluminum resonance at 992 keV how the energy at the peak yield, E_P, is related to the resonance energy E_R, to target thickness t, and to spreading factors W_F, as determined from the calculated curves in Figs. 3 and 4. If E_R is to be determined accurately, however, experimental target conditions must approach the ideal conditions assumed for Figs. 2 and 3.

CONCLUSIONS

Results of this work show that a number of processes enter to determine the form of experimental resonance yield curves. Many problems are presented by these results and few are satisfactorily solved. Perhaps the most serious shortcoming of the calculations is the strict use of the $1/Q^2$ law between $Q_{\max}$ and $Q_{\min}$ for energy losses. This is recognized as a crude approximation for low Q values. The authors feel that attempts to determine a more realistic expression may not be useful until experimental results are improved.

Extension of the experimental work to many resonances in many materials may not be rewarding until the target environment is greatly improved. Pressures in the target chamber of 10^{-10} mm-Hg may be needed. Solid-state effects may enter, and target preparation methods must be studied.

In resonance energy determinations, results up to the present are probably most useful in showing shortcomings of previous practice. Shifts of the half-plateau position from the resonance position in thick-target yield curves can be substantial, but the corrections as given in Fig. 22 apply to only one resonance, and even here they cannot be safely applied unless actual target conditions are similar to those assumed in the calculations. One of the safer procedures for energy calibration work may be the use of targets thin compared to the combined spreading factors, including nuclear resonance width, Doppler width, and beam energy spread.

As yet, no effort has been made to study effects of processes described here on the shape of threshold curves. This will be done soon.[12]

ACKNOWLEDGMENT

The authors wish to express appreciation to Professor C. H. Blanchard for many helpful discussions concerning material in the Appendixes.

APPENDIX A. DERIVATION OF EQUATION (4)

It may be assumed that $W(E_i,E,x)$ depends only on E_i-E and x, and that $g(E_B,E_i)$ depends only on E_B-E_i. If we recognize, further, that $W(E_i-E,x)$ vanishes for $E_i<E$, then the lower limit on the E_i integration in Eq. (1) may be replaced by E giving

$$Y(E_B,t)=N\int_0^\infty dE\,\sigma(E)\int_E^\infty dE_i\,g(E_B-E_i)\times\int_0^t dx\,W(E_i-E,x)n(x). \quad (5)$$

Now since $W(E_i-E,x)$ gives the energy distribution at depth x for particles entering the target at energy E_i, then, in the limit as target thickness goes to zero, we

[12] A preprint of work by P. O. Bondelid and J. W. Butler was received soon after submission of this paper. Results from a thesis by Keith Symon (Harvard, Ph.D., 1948) are used by Bondelid and Butler to fit their experimental data. This analysis, to be accurate for any target, thick or thin, requires distribution functions that are accurate for very thin films and at 1-MeV energy. Symon's results are not valid under these conditions, as he clearly states. Improved accuracy should be attainable by use of the extensions to Symon's results as worked out by Walter Rosenzweig [Phys. Rev. **115**, 1683 (1959)] but they will be only qualitatively correct for this application. Results of H. W. Lewis [*ibid.* **125**, 937 (1962)] or the Monte Carlo method are believed to be accurate within the limits of applicability of the $1/Q^2$ law for energy loss.

have for energy dependence

$$\lim_{t\to 0}\int_0^t dx\, W(E_i-E,x)n(x)\propto\delta(E_i-E), \tag{6}$$

where $\delta(E_i-E)$ is a Dirac delta function. Thus, the yield for a target of infinitesimal thickness can be written

$$Y(E_B,0)\propto N\int_0^\infty dE\,\sigma(E)\int_0^\infty dE_i\, g(E_B-E_i)\delta(E_i-E), \tag{7}$$

or

$$Y(E_B,0)\propto N\int_0^\infty dE\,\sigma(E)g(E_B-E). \tag{8}$$

Defining $\epsilon=E_i-E$ and changing the order of integration in Eq. (5) we obtain

$$Y(E_B,t)=N\int_0^\infty d\epsilon\int_0^\infty dE\,\sigma(E)g[(E_B-\epsilon)-E]\times\int_0^t dx\, W(\epsilon,x)n(x). \tag{9}$$

Combining Eqs. (8) and (9) we obtain

$$Y(E_B,t)\propto N\int_0^\infty d\epsilon\, Y(E_B-\epsilon,0)\int_0^t dx\, W(\epsilon,x)n(x). \tag{10}$$

APPENDIX B. AREA THEOREM

Equation (1) gives the number of resonance reactions produced by N particles incident on a target of thickness t. If E_B is allowed to vary from 0 to ∞, then the area per particle under the resulting yield curve may be written

$$A_t=\int_0^\infty dE\,\sigma(E)\int_0^t dx\, n(x)\int_0^\infty dE_i\, W(E_i-E,x)\times\int_0^\infty dE_B\, g(E_B-E_i), \tag{11}$$

where the beam spread is assumed independent of E_B, and W is assumed to depend on E_i-E and x. Since the area under $g(E_B-E_i)$ is normalized to unity, Eq. (11) becomes

$$A_t=\int_0^\infty dE\,\sigma(E)\int_0^t dx\, n(x)\int_0^\infty dE_i\, W(E_i-E,x). \tag{12}$$

Further simplification results upon recognizing that all particles pass through a slab in the target at any depth x, which requires that $\int dE_i\, W(E_i-E,x)=1$. Thus, the area per particle becomes

$$A_t=\int_0^\infty dE\,\sigma(E)\int_0^t dx\, n(x), \tag{13}$$

where $\int dE\sigma(E)$ is constant for a given resonance, and $\int_0^t dx\, n(x)$ gives the number of disintegrable nuclei/cm^2 for a target of constant thickness. For targets of varying thickness, this must be averaged over the surface of the target.

In words, Eq. (13) states that for a given resonance, the area under the yield curve depends only on the number of disintegrable nuclei/cm^2 averaged over the target surface; other target conditions such as contamination and nonuniform thickness affect the shape of the yield curve, but not the area under it.

No assumptions are made above concerning the nature of the energy losses suffered by a particle as it passes through the target. Hence, the area under the yield curve is independent of the stopping power of the material and is independent of the nature of the energy-loss process.

APPENDIX C. TARGET THICKNESS

Consider a pure target of uniform thickness t_p and with n_p nuclei/cm^3. The area per particle under the yield curve is, from Eq. (13),

$$A_{t_p}=n_p t_p\int_0^\infty dE\,\sigma(E). \tag{14}$$

Since $\int dE\, W(E_i-E,x)=1$, then for $E\ll E_i$ it can be shown that as target thickness goes to infinity

$$\lim_{t_p\to\infty}\int_0^{t_p} dx\, W(E_i-E,x)=1/k, \tag{15}$$

where k is the stopping power of the target.[13] So, for an infinitely thick, pure target, Eqs. (5) and (15) give for the plateau yield per particle

$$Y_p(\infty,\infty)=\frac{n_p}{k}\int_0^\infty dE\,\sigma(E), \tag{16}$$

where the normalization of $g(E_B-E)$ has been used. By eliminating $\int dE\,\sigma(E)$ between Eqs. (14) and (16), one obtains for the uniform thickness of pure target needed to produce area A_{t_p}

$$t_p=A_{t_p}/kY_p(\infty,\infty). \tag{17}$$

According to Appendix B, the area under a yield curve does not depend directly on the target shape or the amount and the distribution of contamination in the target. Thus, to each experimental target which produces a yield curve with area A, there may be associated a pure target, with uniform thickness t_p determined from Eq. (17) by setting $A_{t_p}=A$. The experimental and associated targets, therefore, produce yield curves with the same area. By referring to Eq. (13), this is seen to demand that both targets have the same number of disintegrable nuclei/cm^2 averaged over the target surface.

[13] H. W. Lewis, Phys. Rev. **125**, 937 (1962).